Published in final edited form as:
*Traffic*. 2010 May ; 11(5): 706–720. doi:10.1111/j.1600-0854.2010.01042.x.

# AMN Directs Endocytosis of the Intrinsic Factor-Vitamin $B_{12}$ Receptor Cubam by Engaging ARH or Dab2

**Gitte Albinus Pedersen**[1,†], **Souvik Chakraborty**[2,†], **Amie L. Stinhauser**[2], **Linton M. Traub**[2], and **Mette Madsen**[1,*]

[1] Department of Medical Biochemistry, University of Aarhus, Ole Worms Allé, Bldg. 1170-1171, DK-8000 Aarhus C, Denmark

[2] Department of Cell Biology and Physiology, University of Pittsburgh School of Medicine, Pittsburgh, PA 15213, USA

## Abstract

Cubam is a multi-ligand receptor involved in dietary uptake of intrinsic factor-vitamin B12 in the small intestine and reabsorption of various low-molecular-weight proteins (such as albumin, transferrin, apolipoprotein A-I and vitamin D-binding protein) in the kidney. Cubam is composed of two proteins: cubilin and amnionless. Cubilin harbors ligand binding capabilities, while amnionless provides membrane anchorage and potential endocytic capacity via two FXNPXF signals within the cytosolic domain. These signals are similar to the FXNPXY signals found in members of the low-density lipoprotein receptor superfamily, which associate with clathrin-associated sorting proteins, including Disabled-2 (Dab2) and autosomal recessive hypercholesterolemia (ARH), during endocytosis. We therefore investigated the functionality of each amnionless FXNPXF signal and their respective interaction with sorting proteins. By sequential mutation and expression of a panel of amnionless mutants combined with yeast two-hybrid analyses, we demonstrate that the signals are functionally redundant and both are able to mediate endocytosis of cubam through interaction with Dab2 and ARH.

### Keywords

amnionless; ARH; clathrin; cubilin; Dab2; endocytosis; [FY]NPX[FY] sorting signal; internalization; receptor; vitamin $B_{12}$

The intrinsic factor (IF)-vitamin $B_{12}$ receptor, cubam, is a complex of two proteins, cubilin and amnionless (AMN) (1). Cubam is a multi-ligand receptor complex expressed in a variety of tissues, including ileum, kidney and yolk sac (2–4). In the ileum, the only known function of cubam is to facilitate uptake of dietary vitamin B12 in complex with its transport protein, IF. In the proximal tubules of the kidney, cubam is involved in reabsorption of various proteins from the glomerular ultrafiltrate (for example albumin, transferrin, apolipoprotein A–I and vitamin D-binding protein), thereby reducing proteinuria (5–8). The cubam complex has been shown to play an important role during fetal development in rodents (2,4), but presently its role in the human yolk sac is unclear.

Cubilin is an ~460-kDa protein composed of a short N-terminal region followed by eight epidermal growth factor (EGF)-like repeats and 27 contiguous CUB domains (9,10). The cubilin protein includes no identifiable transmembrane region or classical signals for

*Correspondence: Mette Madsen, mette@biokemi.au.dk.
†These authors contributed equally to this study.

endocytosis. These features are, however, found in the other cubam partner, AMN, which is an ~45-kDa type I transmembrane protein containing two putative internalization signals of the FXNPXF type within its cytosolic domain (1,11,12). This type of signal closely resembles the FXNPXY signal found in receptors of the low-density lipoprotein (LDL) receptor superfamily (13). FXNPX[YF] signals are known to be involved in endocytosis through clathrin-coated buds by binding to specific adaptor proteins (14,15). FXNPXY signals have been shown to mediate endocytosis through interaction with clathrin-associated sorting proteins (CLASPs) harboring phosphotyrosine-binding (PTB) domains (16). The CLASPs Disabled-2 (Dab2) and autosomal recessive hypercholesterolemia (ARH, also termed LDLRAP1) have both been reported to interact with FXNPXY signals. They mediate internalization of the LDL receptor, megalin and low-density lipoprotein receptor related protein (LRP) (17–22). The FXNPXF signal found in AMN is relatively rare, but as demonstrated by Brown and Goldstein, the anchor tyrosine can be exchanged for a phenylalanine without loss of function (23). We therefore investigated if Dab2 and/or ARH can interact with the signals in AMN as well.

In the present study, we show that both AMN FXNPXF signals are active in terms of internalization of cubam and cubam ligands. The signals are functionally redundant, and we demonstrate that internalization of cubam is dependent on interchangeable binding to ARH or Dab2. We propose that AMN directs internalization of the IF-vitamin $B_{12}$ receptor complex, cubam, by engaging ARH and/or Dab2.

## Results

### FXNPXF signals in AMN mediate internalization of cubam

To investigate the importance of the two putative FXNPXF endocytic signals within the cytosolic domain of AMN, we expressed wild-type (WT) and mutated AMN-myc constructs encoding mutations in signal I (amino acid residues 406–411 of human AMN), signal II (amino acid residues 441–446 of human AMN) or both signals in a mammalian expression system, also expressing a truncated cubilin minireceptor (truncated after CUB domain 8) (Figure 1). A chinese hamster ovary (CHO-K1) cell line that neither expresses cubilin nor AMN endogenously was used. Cell lines were designated as follows: WT, I−II+ (first signal eliminated), I+II− (second signal eliminated) and I−II− (both signals eliminated). Immunofluorescent staining of these four cell lines showed that cubilin and AMN were present at the cell surface in all cells (Figure 2). Staining of total levels of cubilin and AMN is found in Figure S1. Because the cubilin minireceptor, if expressed in the absense of AMN, is retained inside the cell in endoplasmic reticulum (ER) or Golgi (1)because of its AMN-dependence during processing from ER and Golgi to the cell surface (4,24,25), and because cubilin contains no transmembrane segment and therefore needs the transmembrane region of AMN to be anchored in the plasma membrane, this demonstrated that the processing of the cubam complex to the cell surface and surface levels of cubam were not affected by mutations in the cytosolic domain of AMN. Furthermore, the interaction between cubilin and AMN appeared not to be affected by the mutations in AMN either, as pull-down experiments with cell lysate of the four cell lines and IF-B12-coupled beads showed that both WT and each of the mutated forms of AMN were coprecipitated with cubilin indicating no differences in binding to cubilin (data not shown). Uptake of $^{125}$I-IF-$B_{12}$ in the four cell lines as well as in single-transfected cubilin minireceptor-expressing cells was studied by continued incubation of cells with $^{125}$I-IF-$B_{12}$ and subsequent measurement of degraded and cell-associated ligand (Figure 3). WT, I−II+ and I+II− cells displayed comparable amounts of degraded $^{125}$I-IF-$B_{12}$, whereas a significantly lower amount of $^{125}$I-IF-$B_{12}$ was degraded in the I II cells (Figure 3A, panel 1). Cell-associated $^{125}$I-IF-$B_{12}$ (representing membrane-bound and internalized but not yet degraded $^{125}$I-IF-$B_{12}$) was increased in the I−II− cells (Figure 3A, panel 3). The observed

differences were most prominent after 8 h of incubation with $^{125}$I-IF-B12, where substantially lower amounts of $^{125}$I-IF-$B_{12}$ was degraded in the I II cells, and an increase in cell-associated $^{125}$I-IF-$B_{12}$ in I II cells compared to WT, I−II+ and I+II− cells was observed (Figure 3B, left panel). Addition of the lysosomal inhibitors, chloroquine and leupeptin, completely inhibited lysosomal degradation of $^{125}$I-IF-$B_{12}$ in all cell lines (Figure 3A, panel 2), while there was an overall increase in cell-associated $^{125}$I-IF-$B_{12}$ because of a build-up of non-degraded ligand within the cells (Figure 3A, panel 4, and 3B, right panel), as previously shown (1). These data show that both FXNPXF signals in the cytosolic domain of AMN possess endocytic capabilities and that one signal is sufficient for uptake of labeled ligand via the cubam complex.

## IF-B12is arrested at the cell surface in I−II− cells

To investigate if the decreased amount of degraded $^{125}$I-IF-$B_{12}$ observed in the I−II− cells was because of impaired internalization, we measured and compared the amount of membrane-bound $^{125}$I-IF-$B_{12}$ at the cell surface in WT and I−II− cells after 8 h of incubation with ligand. Cells were washed with ethylenediaminetetraacetic acid (EDTA) after 8 h of incubation with $^{125}$I-IF-$B_{12}$ disrupting the calcium-dependent binding to cubam, and cell-associated radioactivity of EDTA-treated cells was compared with that of untreated cells (Figure 4A). In the I−II− cells almost 55% of the cell-associated $^{125}$I-IF-$B_{12}$ was present at the cell surface after 8 h, while only 5% was present at the cell surface of WT cells after 8 h. This indicates that IF-$B_{12}$ stays bound at the cell surface much longer in I−II− cells than in WT cells, confirming that the decreased degradation of $^{125}$I-IF-$B_{12}$ in I−II− cells is because of a low internalization rate.

In addition, the internalization in WT and I−II− cells was studied by immunofluorescence microscopy. Cells were incubated with anti-cubilin antibodies for 1 h at 4°C to allow binding to cubilin, washed, and then incubated at 37°C to allow internalization. After 0 and 30 min of incubation at 37°C, the cells were fixed and stained with secondary Alexa 488 conjugated antibodies and 4, 6′-diamidino-2-phenylindole (DAPI) (Figure 4B). As expected, surface labeling of cubilin was observed in both cell lines at 0 min. After 30 min of incubation at 37°C, cubilin had been cleared from the cell surface and a strong intracellular staining of cubilin was observed in the WT cells indicating that the cubam complex had been internalized. In the I−II− cells, however, the cubilin staining was similar to the 0 min-staining, indicating that most of the cubam complex was still present at the cell surface and had not been internalized yet. Similarly, the internalization of IF-$B_{12}$ via the cubam complex in WT and I−II− cells was studied (Figure S2). Both experiments demonstrate that the internalization of cubam is mediated by AMN using its FXNPXF signals.

## An autonomous and transplantable sorting signal in the AMN cytosolic domain

To ascertain whether the cytosolic domain of AMN has an autonomous and transplantable internalization signal (and to rule out any effect of the tandem C-terminal c-myc tag), we generated chimeras with the extracellular and lumenal domain of Tac, the αchain of the IL-2 receptor (CD25) (26). After incubating HeLa cells transiently expressing Tac with anti-Tac antibodies on ice, the membrane-embedded reporter was diffusely distributed over the surface of the cell, and was also present at the extreme periphery, in filopodial extensions (Figure 5A). Upon heating to 37°C, little change in the overall localization of Tac was evident (Figure 5B), confirming that this plasma membrane reporter undergoes extremely slow internalization (26,27). Addition of the murine AMN cytosolic domain (residues 381–459) to the Tac reporter resulted in obvious clustering of the transmembrane protein at numerous puncta apparently randomly positioned over the adherent surface of the transfected cells (Figure 5C). In the cold, the localization of the anti-Tac antibody to the surface spots was most clearly seen in low-expressing cells. After a short 37°C chase, the

antibody-labelled Tac-AMN cleared off the cell surface and was then seen in larger, internal early endosomes (Figure 5D). An F413A substitution in the context of the Tac-AMN (381–459) chimera (Figure 5E,F), or truncation of signal II (381–418) (Figure 5G,H), still allowed robust internalization upon heating to 37°C. Simultaneous mutation of both signal I and signal II (F413A/F451A in Tac-AMN (381–459)) clearly disrupted endocytosis of the reporter. When labeled on ice with anti-Tac, the F413A/F451A mutant was no longer clustered in puncta (Figure 5I) and moved off the surface into endosomes only slowly; although there was some endosomal labeling, compared with the Tac construct not fused to AMN (Figure 5B), the bulk of the signal I/II mutant remained on the cell surface (Figure 5J). These morphologic results are in good accord with the uptake data (Figures 3, 4 and S2) and reiterate the functional redundancy between the two FXNPXF signals in the AMN cytosolic domain.

To verify that the surface puncta in which the Tac-AMN accumulates correspond to sites of clathrin-mediated endocytosis, we compared the localization of the transfected reporter with the LDL receptor. On ice, both transmembrane proteins colocalized to a high degree at patches on the basal surface of HeLa cells (Figure 6A–C). The patches of cell surface-associated Tac-AMN also colocalized with the β2 subunit of the AP-2 adaptor complex (Figure 6D–F). After heating to 37°C, the Tac-AMN trafficked into transferrin-positive endosomes (Figure 6G–I), which represents an archetypical clathrin-mediated sorting itinerary. Because the two FXNPXF signals in AMN closely resemble the FXNPXY signal found in the LDL-receptor superfamily, this suggests that AMN might utilize the same clathrin-associated PTB-domain CLASPs for internalization as the LDL receptor (28–30).

## Recognition of the FXNPXF signal by the clathrin sorting machinery

In nature, a phenylalanine side chain in place of the terminaltyrosine of an FXNXPY signal is rare (14,15), although such a substitution probably has little functional consequence, as observed for the Y807F substitution in the LDL receptor (23,31). Yet, the pair of FXNPXF sequences is highly conserved in AMN orthologues through evolution (Figure 7A). In oviparous vertebrates, the distal signal II is [FY]XNP[LV]Y, but is F[VL]NPLF in mammals (Figure 7A). Remarkably, outside of the signals I and II, there is much phylogenetic divergence in sequence of the cytosolic domain of AMN, suggesting that the major functional attributes of this domain are these internalization signals.

To establish experimentally whether the AMN FXNPXF signals bind physically to the PTB domain in sorting adaptors, we performed a yeast two-hybrid screen. On both triple and quadruple dropout selective media plates, ARH interacted strongly with the AMN cytosolic domain and the transformed Saccharomyces cerevisiae AH109 cells grew vigorously (Figure 7B). If co-transformed with the AMN cytosolic domain and Dab2 PTB domain, the AH109 cells grew less robustly, however. An F413A substitution disrupting signal I had little effect on the interaction with either ARH or the Dab2 PTB domain, but inactivation of both signals (F413A/F451A double mutant) abolished growth. This indicates that both the Dab2 and ARH PTB domains can engage the signal II FVNPLF sequence. We therefore removed signal II by truncating the AMN cytosolic domain to residue 418. This prevented growth in yeast co-transformed with the Dab2 PTB domain (introducing an F413Y mutation in AMN 381–418 did not rescue interaction with Dab2 PTB), whereas the AMN 381–418 fragment still interacted with ARH, albeit more weakly than the entire cytosolic domain did. This interaction with ARH was disrupted by mutation of F413 to alanine in AMN 381–418. Further truncation removing signal I (AMN 381–400) prevented growth of all co-transformed AH109. Together, these interaction screen data suggest that both PTB-domain CLASPs can bind to AMN. ARH can engage both signal I and signal II, although signal II must evidently be present in the context of the entire cytosolic domain, as ARH did not bind

to the truncated AMN fragment consisting of residues 427–458. Dab2 seems to recognize the distal signal II preferentially and accordingly bound the 427–458 fragment.

Next, we investigated the role of ARH and Dab2 in Tac-AMN endocytosis in a mammalian model system using short interfering RNA (siRNA) silencing (29). HeLa SS6 cells were either mock siRNA transfected or transfected with specific siRNA duplexes targeting ARH and/or Dab2 mRNA. After 24 h, siRNA-treated cells were transfected with Tac-AMN while mock-transfected cells were co-transfected with Tac-AMN and tdRFP to allow facile discrimination of the two populations of cells. After the second series of transfections, mock-and siRNA-treated cells were cocultured, and subsequently labeled. In mock siRNA-treated HeLa cells labeled on ice with anti-Tac antibodies, the typical clustered punctate pattern was observed (Figure 8B–D). The distribution of the Tac-AMN was indistinguishable in cells where either ARH (Figure 8B) or Dab2 (Figure 8C) alone had been effectively depleted (Figure 8A). In addition, the African green monkey-derived BS-C-1 cell line (32) has very weak relative Dab2 expression while displaying normal levels of ARH (Figure 9A) (29). These cells also showed clustering the Tac-AMN reporter at surface puncta (data not shown). Either Dab2 or ARH are therefore able to concentrate the Tac-AMN transmembrane protein at the cell surface.

In dramatic contrast, in cells where both ARH and Dab2 had been simultaneously extinguished, Tac-AMN accumulated over the surface, similar to the distribution of the Tac reporter (Figure 5A). In the adjacent non-knocked-down cells (identified by transfection with tdRFP), clustered Tac-AMN was observed as expected. Upon a 37°C chase, the Tac-AMN passed into subcellular endosomes in ARH or Dab2 siRNA-treated cells (Figure 8E,F), but persisted at the cell surface in cells subjected to ARH and Dab2 RNAi silencing (Figure 8G). The effect on internalization of Tac-AMN of double knockdown of ARH and Dab2 was similar to the effect on internalization of the LDL receptor (Figure 8H–M) (29,30). The remarkable similarity in the behavior of the panel of AMN constructs mutated in both signal I and II or when both ARH and Dab2 are depleted indicates mechanistic linkage.

## Recognition of signal I by Dab2 in vivo

In ARH−/− patient fibroblasts, which express Dab2 strongly (Figure 9A) (33), LDL receptor internalization is intact because of the functional redundancy between ARH and Dab2 (28–30). As anticipated, in ARH-nullizygous fibroblasts transfected with Tac-AMN (381–459), the surface population of the transmembrane reporter was clustered at puncta (Figure 9C) that were also positive for Dab2 (Figure 9C′), while Tac alone had a dispersed distribution over the entire cell surface (Figure 9B). Because our yeast two-hybrid studies indicated that Dab2 selectively engages the distal FXNPXF signal II within the AMN cytosolic domain, we evaluated the distribution of both a truncated Tac-AMN, lacking signal II (381–418), and the signal II mutant (F451A) transfected into the ARH genetically null cells. In both cases, the Tac-AMN was still clustered at discrete puncta on the bottom surface of the transfected cells, yet the signal I−II− double mutant [F413A/F451A in Tac-AMN (381–459)] was largely diffusely distributed over the cell surface (Figure 9D–F), similar to Tac (Figure 9B). This indicates that in these cells the clustering of the Tac-AMN chimeras was still dependent upon the tandem FXNPXF motifs. Essentially similar results were obtained using two different ARH−/− cell lines derived from unrelated patients (34,35). These data indicate that in the context of assembled clathrin-coated structures, Dab2 can engage the proximal AMN signal I FXNPXF sequence.

This conclusion is supported by siRNA experiments in HeLa SS6 cells, where both the truncated [Tac-AMN (381–418)] and signal II-mutated Tac-AMN (F451A) reporters were concentrated at surface puncta in cells treated with a SMART pool of ARH silencing siRNA

duplexes (Figure 9G–L). Moreover, like the Tac-AMN protein, both the Tac-AMN (381–418) and the F451A mutants were internalized into peripheral endosomes within 10 min at 37°C (Figure 9I–M), unlike the F413A/F451A double mutant (Figure 9O). Together, the results indicate that Dab2 can recognize the proximal FXNPXF signal in the AMN cytosolic domain in clathrin-coated buds.

## Discussion

A general feature of clathrin-mediated endocytosis is the use of structurally distinct sorting signals to prevent competition for entry of different transmembrane proteins (36,37). The diversity of signals allows unrelated cargo molecules to be concentrated together within incipient clathrin-coated structures, and also allows stimulus-dependent clearance of membrane-embedded proteins in the face of ongoing constitutive internalization (14,15,38). The principal clathrin adaptor at the plasma membrane, AP-2, recognizes two distinct sorting signals, the YXXØ and [DE]XXXL[LIM]-type sequences (39–42). Yet, other signals, like phosphorylation, ubiquination and the FXNXP[YF] sequence, are decoded by CLASPs that directly contact AP-2 (15,43–45). We show here that the transmembrane partner of the cubam receptor complex, AMN, via its two apparently functionally redundant FXNPXF signals promotes clathrin-dependent internalization utilizing the CLASPs ARH or Dab2. In this way, AMN mediates uptake of cubam ligands.

Our data indicate that ARH or Dab2 alone or together are able to direct uptake of the cubam complex and its ligands, which is in accord with descriptions of overlapping expression patterns and functions of Dab2 and ARH in model animals. In zebrafish, similar expression patterns for cubam, megalin, Dab2 and ARH or relevant zebrafish homologs either in the adult or the fetal zebrafish are observed (46,47). The same is found in mice, where cubam, megalin, Dab2 and ARH are all expressed in the kidney proximal tubule positioned at the apical plasma membrane (unpublished observations). An excellent case of the proposed overlapping function is exemplified in the fetal mouse, where Dab2 expression in the yolk sac, a polarized extraembryonic epithelium required for nutrient uptake from the adjacent uterine tissue and lacking ARH expression, is sufficient for proper function of cubamand megalin (4,18). Accordingly, Arh−/− animals do not display any overt developmental abnormalities (48), whereas Dab2 function can not be substituted for by ARH in the yolk sac. Consequently, Dab2 nullizygous fetuses die at an early gastrulation stage (18,49)indicating the critical role of Dab2-dependent systems, including cubam and megalin, during transfer of nutrients from the adjacent uterine tissue to the growing fetus during rodent development.

While our siRNA experiments in HeLa cells reveal functional redundancy between Dab2 and ARH, essentially analogous to the sorting of the LDL receptor (28–30), AMN typically operates in vivo at the apical surface of polarized epithelia (1,4,25). In this regard, the differences we note between ARH and Dab2 binding to the AMN cytosolic domain, and the selection for tandem phenylalanine-containing FXNPXF sequences may be relevant. Invertebrate genomes encode AMN-like proteins [TreeFam (www.treefam.org/) accession number TF323790] (50), and in several Drosophila species as well as Culex quinquefasciatus and Aedes aegypti mosquitoes, a single F[DN]NPMF signal is present within the putative cytosolic domain of AMN homologs. However, in Anopheles gambiae (FNNPMY), the wasp Nasonia vitripennis (FENPLY), and the aphid Acyrthosiphon pisum (FDNPTY) a terminal tyrosine is present. So, in insects, both FXNXPF and FXNXPY signals are represented in AMN-like proteins. In Ornithorhynchus anatinus, the platypus, signal I (FVNPVF) and signal II (FDNPMF) both have a phenylalanine anchor residue. As monotremes diverged from therian mammals over 160 million years ago (51), and mammalian AMN signals I and II are both of the FXNPXF type, this demonstrates a

remarkable selection pressure on AMN to retain the terminal phenylalanines despite substantial variation (including deletions) within the remainder of the cytoplasmic domain (Figure 7A).

The variable length of the AMN cytosolic domain in vertebrates and the different relative spacing between signals I and II suggest that an optimal positioning of the sorting sequence relative to the inner leaflet of the bilayer, as is seen in LAMPs for example (52), does not seem to be necessary. Perhaps two signals are needed to attach bivalently to a pair of PTB-domain CLASPs during uptake to enhance the apparent affinity. In the kidney proximal tubule, where megalin is a major and abundant scavenger receptor that might compete with cubam for occupancy of limited amounts of Dab2 or ARH within assembling clathrin-coated buds, tandem signals may ensure packaging of the cubam complex despite a heavy load of megalin traffic. Alternatively, the higher apparent affinity of AMN for ARH noted in the two-hybrid screen may be indicative of an in vivo preference for this PTB-domain CLASP in the appropriate epithelial tissue type. Currently, the relative stoichiometry of Dab2 and ARH in either small intestine (enterocytes) or the nephron (proximal tubule) is unknown. There are Expressed Sequence Tag (EST) ESTs for each CLASP derived from both tissues in humans and mice. A higher apparent affinity for AMN may drive partitioning of ARH into clathrin-coated vesicles forming at the apical plasma membrane. Ultrastructural studies show that megalin−/− kidney proximal tubule displays a dramatic reduction in clathrin-coated structures at the crypts of apical microvilli (53). Analogously, Dab2−/− mice display a prominent change in the steady-state positioning of megalin to the brush border (54), and also have decreased clathrin-coated vesicles and accompanying proteinuria (49). This suggests that Dab2, which binds physically to clathrin and alone is able to promote the assembly of spherical clathrin assemblies in vitro (55), may be a major inducer of clathrin-coat assembly at the apical plasma membrane of these cells. By selectively binding to ARH, which uses a privileged AP-2 binding surface upon the AP-2 β2 subunit appendage (56–58), AMN may also be accommodated within forming vesicles. In fact, the reported dependence of cubilin uptake on megalin (6) might be a reflection of the vital role that a megalin–Dab2 interaction plays in the general construction of clathrin-coated vesicles at the apical surface rather than signifying that megalin is directly responsible for cubilin uptake. Importantly, the lethal effect of targeted gene disruption of Dab2 in mice is consistent with a specialized role for ARH in cubam internalization in the kidney proximal tubule or small intestine, as ARH immunoreactivity is not detectable in the visceral endoderm (18). Similarly, unfortunate individuals bearing two mutant ARH alleles present with hypercholesterolemia clinically analogous to familial hypercholesterolemia because of loss of LDL receptor function (59), as Dab2 levels in hepatocytes are very low (29) leaving the LDL receptor dependent upon ARH. Thus, reduced or absent expression of either Dab2 or ARH in certain tissues may be accounted for by the functional redundancy of some FXNPX[YF]-containing receptors, including AMN.

The renal outer medullary potassium (ROMK) channel was just recently reported to use a 373YXNPXFV sequence for ARH-dependent uptake (60). Interestingly, this signal also contains a C-terminal phenylalanine anchor as opposed to the typical tyrosine. Apparently fully selective for the ARH PTB domain over that of Dab2, numb, or GULP/Ced-6, the distal valine residue seems to be as important for ARH binding as the preceding tyrosine, asparagine and phenylalanine anchor residues of the sorting signal (60). Neither of the AMN FXNPXF signals are followed by a valine residue (Figure 7A); the only hydrophobic side chain present is a tyrosine following the phenylalanine at the Bos taurus signal I (Figure 7A). Also, while the ROMK ARH-specific YDNPNFV has a tyrosine residue leading the signal, almost all AMN endocytic signals begin with a phenylalanine. Although the recognition consequence of a Y373F or F378Y substitution was not evaluated for ROMK (60), the subtle differences/degeneracy between the different sequences may make the AMN

signals I and II able to engage the ARH and Dab2 PTB domains unlike the ROMK YXNPXFV sequence.

## Materials and Methods

Anti-cubilin: polyclonal anti-rat cubilin antibody raised in rabbits (at DAKO, Copenhagen, Denmark) against IF-$B_{12}$-affinity chromatography-purified CHO-K1 cell-produced recombinant rat cubilin protein (amino acids R110-H1369), and rabbit polyclonal anti-rat cubilin antibody (previously used and described in 10). Monoclonal alkaline phosphatase-conjugated anti-myc antibody (Invitrogen). Monoclonal anti-human amnionless antibody (R&D Systems). Anti-clathrin heavy chain monoclonal antibody (mAb) (61). AP-1/2 β1/β2 subunit mAb 100/1 (62). Affinity-purified anti-Dab2 and anti-ARH polyclonal antibodies (55). Affinity-purified anti-AP-1/2 β1/β2 subunit antibody GD/1 (63). Anti-LDLR mAb IgG-C7 (55). Purified anti-CD25 (anti-Tac) mAb (Ancell). Rabbit polyclonal anti-Tac antibody generously provided by Juan Bonifacino (NIH, Bethesda, MD). Alexa dye-conjugated secondary antibodies (Molecular Probes).

Human and porcine IF-$B_{12}$ purified from gastric mucosa as well as anti-human IF antibody was generously provided by Dr. Ebba Nexø (Aarhus University Hospital, Denmark). Recombinant human IF-$B_{12}$ produced in yeast was generously provided by Dr. Gregers Rom Andersen (Centre for Structural Biology, University of Aarhus, Denmark).

### Plasmids for expression of recombinant AMN

The two presumptive internalization signals in human AMN were designated signal I (amino acid residues 406–411) and signal II (amino acid residues 441–446). Three cDNA constructs were synthesized with the first (I−II+), the second (I+II−) or both (I−II−) signals mutated (Figure 1B). I−II+, I+II−, and I−II− AMN cDNA constructs were generated using the site-directed ligase-independent mutagenesis (SLIM) method (64). Polymerase chain reaction (PCR) was performed using a previously described human WT AMN cDNA-construct C-terminally tagged with five c-myc tags (1) as first template. PCR products were subjected to DpnI digestion of the template strands and hybridized by repeated melting and annealing to obtain hetero duplexes prior to transformation. Tac in pcDNA3 was generously provided by Rebecca Hughey (University of Pittsburgh, Pittsburgh, PA, USA). Cytosolic domain of murine AMN (amino acid residues 381–459 or 381–418) was fused in-frame to the C-terminus of Tac. The adjacent XhoI and NotI sites in pcDNA3-Tac were used for subcloning. Tac-AMN F413A 381–459 and Tac-AMN F413A/F451A 381–459 mutants were generated with QuickChange site-directed mutagenesis. All constructs were verified by automated dideoxynucleotide sequencing, and the details of primers and sequences are available upon request.

### Short interfering RNA

The siRNA oligonucleotides targeting Dab2 and ARH were obtained from Dharmacon/ThermoFisher Scientific and have been described previously (29). The Dab2 siRNA targets base pairs 745–763 of the Dab2 nucleotide sequence (UUCUUUAAGAGAAAAUCCA) and ARH siRNA targets base pairs 633–651 of the ARH nucleotide sequence (CCUGCUGGACUUAGAGGAG).

### Cell culture and transfections

AMN constructs were transfected into a CHO-K1 cell line previously transfected with a cubilin minireceptor construct (amino acids 1–1389 of rat cubilin) (1) using Dosper Liposomal Transfection Reagent (Roche Diagnostics). Stable double-transfected CHO-K1 clones expressing cubilin and WT, I−II+, I+II−, or I−II− AMN-myc were established by

selection with 1 mg/mL Geneticin (Invitrogen), and cell lines expressing both minicubilin and AMN were cultured in HyQ CCM5 growth medium (HyClone) supplemented with 300 μg/mL Zeocin (Invitrogen) and 500 μg/mL Geneticin. HeLa SS6 cells (65)were cultured in DMEM supplemented with 10% fetal calf serum and 2 mml-glutamine and maintained at 37°C in a humidified atmosphere containing 5% CO2. For transfection, HeLa SS6 cells were seeded onto glass coverslips in 35 mm dish and allowed to attach. Cells were then transfected with 100–500 ng of appropriate mammalian plasmid vector(s). ARH−/− primary fibroblasts (34,35) were cultured as described (33) and transiently transfected with Lipofectamine2000.

For RNAi experiments, HeLa SS6 cells were seeded in 24-well plates and grown to 50% confluence. The cells were then either mock transfected or transfected with 100 nm of siRNA targeting Dab2 and/or ARH using oligofectamine (Invitrogen) as per manufacturer's instructions. After another 24 h, the siRNA-treated cells were transfected with 100 ng of Tac-AMN, while mock-treated cells were co-transfected with 100 ng of Tomato tandem dimer red fluorescent protein (tdRFP) vector and 100 ng of Tac-AMN. Six hours later, the cells were trypsinized and cocultured at 1:1 ratio for another 24 h in a 24-well plate with or without glass coverslips. The cells were then processed for receptor internalization assays (see below) or for electrophoresis and immunoblotting (see below).

### Electrophoresis and immunoblotting

CHO-K1 cells were lysed on ice in PBS buffer (10 mm NaH2PO4, 150 mm NaCl, 6 mm CaCl2) including 1% Triton X-100 (Merck) and Complete mini EDTA-free protease inhibitor cocktail tablets (Roche Diagnostics), pH 7.4. Protein samples were boiled in sample buffer (20 mm Tris, pH 6.8, 5% SDS, 17.4% glycerol and pyronin Y) and tested by nonreducing sodium dodecyl sulphate-polyacrylamide gel electrophoresis (SDS–PAGE) using 8–16% or 4–16% gels. Proteins were blotted onto a polyvinylidene difluoride (PVDF) membrane, and immunoblotting was performed with antibodies (as indicated in figure legends) diluted to 5 μg/mL. Proteins were detected using 5-bromo-4-chloro-3-indolyl-phosphate-nitro blue tetrazolium.

HeLa SS6 cells were lysed using sonication and then heated at 95°C for 5 min. Samples were then resolved on polyacrylamide gels prepared with acrylamide:bisacrylamide (30:0.4) ratio stock solution. After SDS–PAGE, proteins were transferred to nitrocellulose in ice-cold 15.6 mm Tris, 120 mm glycine. Blots were blocked overnight or for 2 h in 5% skim milk in 10 mm Tris–HCl, pH 7.8, 150 mm NaCl, 0.1% Tween-20, and then portions were incubated with primary antibodies as indicated in the figure legends. After incubation with horseradish peroxidase (HRP)-conjugated anti-mouse or anti-rabbit IgG, immunoreactive bands were visualized with enhanced chemiluminescence.

### Immunoprecipitation of cubilin and AMN from cell lysate

Cell lysates from CHO-K1 cells expressing minicubilin and WT, I−II+, I+II− or I−II− AMN-myc were incubated for 2 h at room temperature with GammaBind G Sepharose beads (Amersham) coated with anti-rat cubilin antibody (DAKO) in PBS with 1 mm EDTA, 0.5% Triton X-100 and Complete mini EDTA-free protease inhibitor cocktail tablets, pH 7.2. Precipitated proteins were eluted in sample buffer, subjected to SDS–PAGE followed by immunoblotting, and co-precipitation of AMN was detected using an alkaline phosphatase-conjugated anti-myc antibody.

### Confocal immunofluorescence microscopy

CHO-K1 WT, I+II−, I−II+ and I−II− AMN-myc cells were fixed in 4% formaldehyde and permeabilized in 1× PBS with 0.1% Triton X-100. Cells were stained with 10 μg/mL anti-rat

cubilin and 10 μg/mL anti-myc in 1× PBS with 0.05% Triton X-100 for 1 h at room temperature followed by incubation with Alexa 488 and Alexa 594 in 1× PBS with 0.05% Triton X-100 for 1 h at room temperature. For staining of surface cubilin, cells were stained with 10 μg/mL anti-rat cubilin and 10 μg/mL monoclonal anti-human AMN antibody in HyQ CCM5 medium for 1 h at 4°C, fixed in 4% formaldehyde for 1 h at 4°C followed by staining with Alexa 488 in 1× PBS for 1 h at room temperature. For anti-cubilin antibody internalization experiments and IF-$B_{12}$ internalization experiments, CHO-K1 cells expressing minicubilin and WT or I−II− AMN-myc were grown on cover slips in 24-well plates to approximately 90% confluence. Cells were incubated with 40 μg/mL anti-cubilin antibody or IF-$B_{12}$ in HyQ CCM5 growth medium for 1 h at 4°C to saturate all receptors and were subsequently either transferred to 37°C and continuously incubated with IF-$B_{12}$ for 0, 1, 2, 4 or 8 h or washed and incubated at 37°C for 30 min to allow internalization of bound ligand or antibody, respectively. After the incubation period, cells were washed in PBS and fixed in 4% formaldehyde in 10 mm PBS, pH 7.4. Cells were stained with either Alexa Fluor 488 goat anti-rabbit and DAPI or 10 μg/mL anti-human IF antibody in PBS with 1% fetal calf serum for 1 h at room temperature. For IF-$B_{12}$ internalization experiments, cells were subsequently incubated with secondary antibody: Alexa Fluor 488 goat anti-rabbit (Molecular Probes) for 1 h at room temperature, cover slips were mounted on object glasses using Dako fluorescent mounting medium (DakoCytomation, DAKO A/S).

For experiments involving LDL receptors, HeLa SS6 cells were switched to DMEM supplemented with 10% lipoprotein-deficient serum (LPDS) and 2 mml-glutamine for 24–48 h to upregulate LDLR expression (29), while for experiments involving transferrin, cells were switched to pre-warmed DMEM supplemented with 25 mm Hepes, pH 7.2 and 0.5% BSA (starvation medium) and incubated at 37°C for 1 h prior to experiment. For experiments involving only Tac or Tac-AMN chimeras, the cells were maintained in regular medium. The cells were then switched to ice-cold starvation medium for 1 h at 4°C and then incubated for additional 1 h at 4°C in ice-cold starvation medium containing 25 μg/mL Alexa 568-labelled transferrin or anti-LDL receptor mAb IgG-C7 and/or anti-Tac antibody (monoclonal or polyclonal). The cells were then either fixed with 3.7% formaldehyde in 1× PBS or switched to 37°C for appropriate amount of time to allow ligand-receptor internalization followed by fixation, and processing for immunofluorescence.

For colocalization analysis of Tac-AMN with clathrin-coated structures, following anti-Tac antibody binding at 4°C, cells were permeabilized for 1 min with 25 μg/mL digitonin at 4°C in prechilled 1× assay buffer (25 mm HEPES-KOH pH 7.2, 125 mm potassium acetate, 5 mm magnesium acetate, 2 mm EDTA, 2 mm EGTA, 1 mm DTT), fixed and immunolabelled with affinity-purified anti-AP-1/2 β1/β2 subunit GD/1 antibody, and further processed for immunofluorescence.

Confocal images were captured using a laser scanning confocal unit with a 63× water objective lens [numerical aperture (NA) 1.2; LSM510, Carl Zeiss] attached to an Axiovert microscope (Carl Zeiss) or an Olympus Fluoview 1000 microscope with an PlanApo N (60×/NA 1.42) oil objective. Sequential scanning was performed for acquiring individual emission channels when more than one fluorophor was followed. Data were acquired using lsm or fv10-asw software. The TIFF files were then imported into Adobe Photoshop for minor adjustments to brightness and/or contrast, and assembled with Freehand software.

### Uptake of 125I-IF-$B_{12}$ in CHO-K1 cells

Porcine and human IF-$B_{12}$ was iodinated by the Cloramine T method. The protein was diluted in NaH2PO4 pH 8.0 and incubated with 125I (100 mCi/mL) and chloramine T for 3 min with gentle shaking. The iodination was quenched using Na2S2O5. The mixture was separated on a Sephadex G25 fine column by gel filtration. Eluates were collected and c.p.m

per μL of each fraction was measured using a gamma-counter. The ratio of bound versus unbound 125I was determined by precipitation with 12.5% trichloroacetic acid (TCA). Fractions with a high c.p.m per μL and at least 95% bound 125I were used for uptake experiments. Triplicates of cells were grown to confluence in 24-well plates and incubated for 1, 2, 4 and 8 h at 37°C in growth medium containing 125I-IF-$B_{12}$ (~4000 c.p.m per well) with or without 1.5 mm of the lysosomal inhibitors chloroquine and leupeptin. The medium was removed and precipitated with 12.5% TCA. Counts were collected using a gamma-counter. Cells were washed in PBS, lysed in 0.5 m NaOH and cell-associated radioactivity was measured. For uptake experiments with EDTA, the cells were washed in PBS with 20 mm EDTA prior to lysis, removing surface-bound 125I-IF-B12.

## Supplementary Material

Refer to Web version on PubMed Central for supplementary material.

## Acknowledgments

Technician Gitte Fynbo Biller is thanked for excellent technical assistance. Author Mette Madsen has previously published under the name Mette Kristiansen. The experimental work was financially supported by the Novo Nordisk Foundation, The Lundbeck Foundation, The Danish Medical Research Council and the National Institutes of Health grants R01 DK53249 and a pilot project from the O'Brien Pittsburgh Center for Kidney Research (P30 DK79307).

## References

1. Fyfe JC, Madsen M, Hojrup P, Christensen EI, Tanner SM, De La Chapelle A, He Q, Moestrup SK. The functional cobalamin (vitamin B-12)-intrinsic factor receptor is a novel complex of cubilin and amnionless. Blood. 2004; 103:1573–1579. [PubMed: 14576052]
2. Sahali D, Mulliez N, Chatelet F, Dupuis R, Ronco P, Verroust P. Characterization of a 280-kD protein restricted to the coated pits of the renal brush border and the epithelial cells of the yolk sac. Teratogenic effect of the specific monoclonal antibodies. J Exp Med. 1988; 167:213–218. [PubMed: 2891781]
3. Seetharam B, Christensen EI, Moestrup SK, Hammond TG, Verroust PJ. Identification of rat yolk sac target protein of teratogenic antibodies, gp280, as intrinsic factor-cobalamin receptor. J Clin Invest. 1997; 99:2317–2322. [PubMed: 9153271]
4. Strope S, Rivi R, Metzger T, Manova K, Lacy E. Mouse amnionless, which is required for primitive streak assembly, mediates cell-surface localization and endocytic function of cubilin on visceral endoderm and.
5. Birn H, Fyfe JC, Jacobsen C, Mounier F, Verroust PJ, Orskov H, Willnow TE, Moestrup SK, Christensen EI. Cubilin is an albumin binding protein important for renal tubular albumin reabsorption. J Clin Invest. 2000; 105:1353–1361. [PubMed: 10811843]
6. Kozyraki R, Fyfe J, Verroust PJ, Jacobsen C, Dautry-Varsat A, Gburek J, Willnow TE, Christensen EI, Moestrup SK. Megalin-dependent cubilin-mediated endocytosis is a major pathway for the apical uptake of transferrin in polarized epithelia. Proc Natl Acad Sci U S A. 2001; 98:12491–12496. [PubMed: 11606717]
7. Kozyraki R, Fyfe J, Kristiansen M, Gerdes C, Jacobsen C, Cui S, Christensen EI, Aminoff M, De La Chapelle A, Krahe R, Verroust PJ, Moestrup SK. The intrinsic factor-vitamin B12 receptor, cubilin, is a high-affinity apolipoprotein A–I receptor facilitating endocytosis of high-density lipoprotein. Nat Med. 1999; 5:656–661. [PubMed: 10371504]
8. Nykjaer A, Fyfe JC, Kozyraki R, Leheste JR, Jacobsen C, Nielsen MS, Verroust PJ, Aminoff M, De La Chapelle A, Moestrup SK, Ray R, Gliemann J, Willnow TE, Christensen EI. Cubilin dysfunction causes abnormal metabolism of the steroid hormone 25(OH) vitamin D3. Proc Natl Acad Sci U S A. 2001; 98:13895–13900. [PubMed: 11717447]
9. Kozyraki R, Kristiansen M, Silahtaroglu A, Hansen C, Jacobsen C, Tommerup N, Verroust PJ, Moestrup SK. The human intrinsic factor-vitamin B12 receptor, cubilin: molecular characterization

and chromosomal mapping of the gene to 10p within the autosomal recessive megaloblastic anemia (MGA1) region. Blood. 1998; 91:3593–3600. [PubMed: 9572993]

10. Moestrup SK, Kozyraki R, Kristiansen M, Kaysen JH, Rasmussen HH, Brault D, Pontillon F, Goda FO, Christensen EI, Hammond TG, Verroust PJ. The intrinsic factor-vitamin B12 receptor and target of teratogenic antibodies is a megalin-binding peripheral membrane protein with homology to developmental proteins. J Biol Chem. 1998; 273:5235–5242. [PubMed: 9478979]
11. Kalantry S, Manning S, Haub O, Tomihara-Newberger C, Lee HG, Fangman J, Disteche CM, Manova K, Lacy E. The amnionless gene, essential for mouse gastrulation, encodes a visceral-endoderm-specific protein with an extracellular cysteine-rich domain. Nat Genet. 2001; 27:412–416. [PubMed: 11279523]
12. Tanner SM, Aminoff M, Wright FA, Liyanarachchi S, Kuronen M, Saarinen A, Massika O, Mandel H, Broch H, De La Chapelle A. Amnionless, essential for mouse gastrulation, is mutated in recessive hereditary megaloblastic anemia. Nat Genet. 2003; 33:426–429. [PubMed: 12590260]
13. Chen WJ, Goldstein JL, Brown MS. NPXY, a sequence often found in cytoplasmic tails, is required for coated pit-mediated internalization of the low density lipoprotein receptor. J Biol Chem. 1990; 265:3116–3123. [PubMed: 1968060]
14. Bonifacino JS, Traub LM. Signals for sorting of transmembrane proteins to endosomes and lysosomes. Annu Rev Biochem. 2003; 72:395–447. [PubMed: 12651740]
15. Traub LM. Tickets to ride: selecting cargo for clathrin-regulated internalization. Nat Rev Mol Cell Biol. 2009; 10:583–596. [PubMed: 19696796]
16. Stolt PC, Bock HH. Modulation of lipoprotein receptor functions by intracellular adaptor proteins. Cell Signal. 2006; 18:1560–1571. [PubMed: 16725309]
17. He G, Gupta S, Yi M, Michaely P, Hobbs HH, Cohen JC. ARH is a modular adaptor protein that interacts with the LDL receptor, clathrin, and AP-2. J Biol Chem. 2002; 277:44044–44049. [PubMed: 12221107]
18. Maurer ME, Cooper JA. Endocytosis of megalin by visceral endoderm cells requires the Dab2 adaptor protein. J Cell Sci. 2005; 118:5345–5355. [PubMed: 16263760]
19. Nagai M, Meerloo T, Takeda T, Farquhar MG. The adaptor protein ARH escorts megalin to and through endosomes. Mol Biol Cell. 2003; 14:4984–4996. [PubMed: 14528014]
20. Oleinikov AV, Zhao J, Makker SP. Cytosolic adaptor protein Dab2 is an intracellular ligand of endocytic receptor gp600/megalin. Biochem J. 2000; 347:613–621. [PubMed: 10769163]
21. Mameza MG, Lockard JM, Zamora E, Hillefors M, Lavina ZS, Kaplan BB. Characterization of the adaptor protein ARH expression in the brain and ARH molecular interactions. J Neurochem. 2007; 103:927–941. [PubMed: 17727637]
22. Morris SM, Cooper JA. Disabled-2 colocalizes with the LDLR in clathrin-coated pits and interacts with AP-2. Traffic. 2001; 2:111–123. [PubMed: 11247302]
23. Davis CG, Van Driel IR, Russell DW, Brown MS, Goldstein JL. The low density lipoprotein receptor. Identification of amino acids in cytoplasmic domain required for rapid endocytosis. J Biol Chem. 1987; 262:4075–4082. [PubMed: 3104336]
24. Coudroy G, Gburek J, Kozyraki R, Madsen M, Trugnan G, Moestrup SK, Verroust PJ, Maurice M. Contribution of cubilin and amnionless to processing and membrane targeting of cubilin-amnionless complex. J Am Soc Nephrol. 2005; 16:2330–2337. [PubMed: 15976000]
25. He Q, Madsen M, Kilkenney A, Gregory B, Christensen EI, Vorum H, Højrup P, Schäffer AA, Kirkness EF, Tanner SM, De La Chapelle A, Giger U, Moestrup SK, Fyfe JC. Amnionless function is required for cubilin brush-border expression and intrinsic factor-cobalamin (vitamin B12) absorption in vivo. Blood. 2005; 106:1447–1453. [PubMed: 15845892]
26. Hawryluk MJ, Keyel PA, Mishra SK, Watkins SC, Heuser JE, Traub LM. Epsin 1 is a polyubiquitin-selective clathrin-associated sorting protein. Traffic. 2006; 7:262–281. [PubMed: 16497222]
27. Humphrey JS, Peters PJ, Yuan LC, Bonifacino JS. Localization of TGN38 to the trans-Golgi network: involvement of a cytoplasmic tyrosine-containing sequence. J Cell Biol. 1993; 120:1123–1135. [PubMed: 8436587]

28. Eden ER, Sun XM, Patel DD, Soutar AK. Adaptor protein Disabled-2 modulates low density lipoprotein receptor synthesis in fibroblasts from patients with autosomal recessive hypercholesterolaemia. Hum Mol Gen. 2007; 16:2751–2759. [PubMed: 17761685]
29. Keyel PA, Mishra SK, Roth R, Heuser JE, Watkins SC, Traub LM. A single common portal for clathrin-mediated endocytosis of distinct cargo governed by cargo-selective adaptors. Mol Biol Cell. 2006; 17:4300–4317. [PubMed: 16870701]
30. Maurer ME, Cooper JA. The adaptor protein Dab2 sorts LDL receptors into coated pits independently of AP-2 and ARH. J Cell Sci. 2006; 119:4235–4246. [PubMed: 16984970]
31. Davis CG, Lehrman MA, Russell DW, Anderson RG, Brown MS, Goldstein JL. The J. D. mutation in familial hypercholesterolemia: Amino acid substitution in cytoplasmic domain impedes internalization of LDL receptors. Cell. 1986; 45:15–24. [PubMed: 3955657]
32. Hopps HE, Bernheim BC, Nisalak A, Tjio JH, Smadel JE. Biologic characteristics of a continuous kidney cell line derived from the african green monkey. J Immunol. 1963; 91:416–424. [PubMed: 14071033]
33. Mishra SK, Watkins SC, Traub LM. The autosomal recessive hypercholesterolemia (ARH) protein interfaces directly with the clathrin-coat machinery. Proc Natl Acad Sci U S A. 2002; 99:16099–16104. [PubMed: 12451172]
34. Abera AB, Marais AD, Raal FJ, Leisegang F, Jones S, George P, Henderson HE. Autosomal recessive hypercholesterolaemia: discrimination of ARH protein and LDLR function in the homozygous FH phenotype. Clin Chim Acta. 2007; 378:33–37. [PubMed: 17150201]
35. Garcia CK, Wilund K, Arca M, Zuliani G, Fellin R, Maioli M, Calandra S, Bertolini S, Cossu F, Grishin N, Barnes R, Cohen JC, Hobbs HH. Autosomal recessive hypercholesterolemia caused by mutations in a putative LDL receptor adaptor protein. Science. 2001; 292:1394–1398. [PubMed: 11326085]
36. Warren RA, Green FA, Stenberg PE, Enns CA. Distinct saturable pathways for the endocytosis of different tyrosine motifs. J Biol Chem. 1998; 273:17056–17063. [PubMed: 9642270]
37. Marks MS, Woodruff L, Ohno H, Bonifacino JS. Protein targeting by tyrosine-and di-leucine-based signals: evidence for distinct saturable components. J Cell Biol. 1996; 135:341–354. [PubMed: 8896593]
38. Pandey MS, Harris EN, Weigel JA, Weigel PH. The cytoplasmic domain of the hyaluronan receptor for endocytosis (HARE) contains multiple endocytic motifs targeting coated pit-mediated internalization. J Biol Chem. 2008; 283:21453–21461. [PubMed: 18539600]
39. Kelly BT, McCoy AJ, Spate K, Miller SE, Evans PR, Honing S, Owen DJ. A structural explanation for the binding of endocytic dileucine motifs by the AP2 complex. Nature. 2008; 456:976–979.
40. Ohno H, Stewart J, Fournier MC, Bosshart H, Rhee I, Miyatake S, Saito T, Gallusser A, Kirchhausen T, Bonifacino JS. Interaction of tyrosine-based sorting signals with clathrin-associated proteins. Science. 1995; 269:1872–1875. [PubMed: 7569928]
41. Owen DJ, Evans PR. A structural explanation for the recognition of tyrosine-based endocytotic signals. Science. 1998; 282:1327–1332. [PubMed: 9812899]
42. Collins BM, McCoy AJ, Kent HM, Evans PR, Owen DJ. Molecular architecture and functional model of the endocytic AP2 complex. Cell. 2002; 109:523–535. [PubMed: 12086608]
43. Robinson MS. Adaptable adaptors for coated vesicles. Trends Cell Biol. 2004; 14:167–174. [PubMed: 15066634]
44. Maldonado-Baez L, Wendland B. Endocytic adaptors: recruiters, coordinators and regulators. Trends Cell Biol. 2006; 16:505–513. [PubMed: 16935508]
45. Schmid EM, McMahon HT. Integrating molecular and network biology to decode endocytosis. Nature. 2007; 448:883–888. [PubMed: 17713526]
46. Anzenberger U, Bit-Avragim N, Rohr S, Rudolph F, Dehmel B, Willnow TE, Abdelilah-Seyfried S. Elucidation of megalin/LRP2-dependent endocytic transport processes in the larval zebrafish pronephros. J Cell Sci. 2006; 119:2127–2137. [PubMed: 16638803]
47. Covassin L, Amigo JD, Suzuki K, Teplyuk V, Straubhaar J, Lawson ND. Global analysis of hematopoietic and vascular endothelial gene expression by tissue specific microarray profiling in zebrafish. Dev Biol. 2006; 299:551–562. [PubMed: 16999953]

48. Jones C, Hammer RE, Li WP, Cohen JC, Hobbs HH, Herz J. Normal sorting but defective endocytosis of the low density lipoprotein receptor in mice with autosomal recessive hypercholesterolemia. J Biol Chem. 2003; 278:29024–29030. [PubMed: 12746448]

49. Morris SM, Tallquist MD, Rock CO, Cooper JA. Dual roles for the Dab2 adaptor protein in embryonic development and kidney transport. EMBO J. 2002; 21:1555–1564. [PubMed: 11927540]

50. Ruan J, Li H, Chen Z, Coghlan A, Coin LJ, Guo Y, Hériché JK, Hu Y, Kristiansen K, Li R, Liu T, Moses A, Qin J, Vang S, Vilella AJ, et al. TreeFam: 2008 Update. Nucleic Acids Res. 2008; 36:D735–D740. [PubMed: 18056084]

51. Warren WC, Hillier LW, Marshall Graves JA, Birney E, Ponting CP, Grützner F, Belov K, Miller W, Clarke L, Chinwalla AT, Yang SP, Heger A, Locke DP, Miethke P, Waters PD, et al. Genome analysis of the platypus reveals unique signatures of evolution. Nature. 2008; 453:175–183. [PubMed: 18464734]

52. Rohrer J, Schweizer A, Russell D, Kornfeld S. The targeting of Lamp1 to lysosomes is dependent on the spacing of its cytoplasmic tail tyrosine sorting motif relative to the membrane. J Cell Biol. 1996; 132:565–576. [PubMed: 8647888]

53. Leheste JR, Rolinski B, Vorum H, Hilpert J, Nykjaer A, Jacobsen C, Aucouturier P, Moskaug JO, Otto A, Christensen EI, Willnow TE. Megalin knockout mice as an animal model of low molecular weight proteinuria. Am J Pathol. 1999; 155:1361–1370. [PubMed: 10514418]

54. Nagai J, Christensen EI, Morris SM, Willnow TE, Cooper JA, Nielsen R. Mutually dependent localization of megalin and Dab2 in the renal proximal tubule. Am J Physiol Renal Physiol. 2005; 289:F569–F576. [PubMed: 15870384]

55. Mishra SK, Keyel PA, Hawryluk MJ, Agostinelli NR, Watkins SC, Traub LM. Disabled-2 exhibits the properties of a cargo-selective endocytic clathrin adaptor. EMBO J. 2002; 21:4915–4926. [PubMed: 12234931]

56. Mishra SK, Keyel PA, Edeling MA, Dupin AL, Owen DJ, Traub LM. Functional dissection of an AP-2 β2 appendage-binding sequence within the autosomal recessive hypercholesterolemia protein. J Biol Chem. 2005; 280:19270–19280. [PubMed: 15728179]

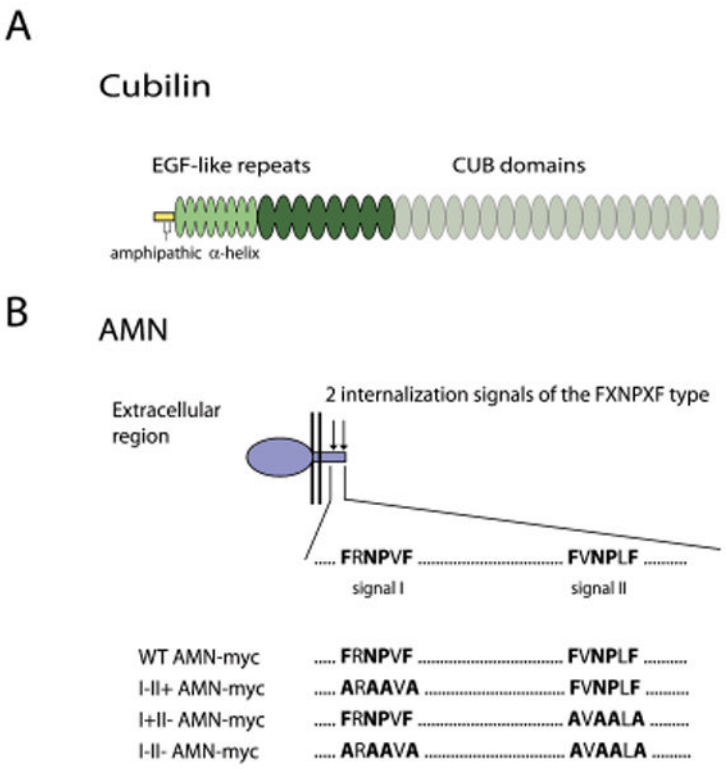


**Figure 1.**

Structure of cubilin and AMN. A) Schematic presentation of the structure of cubilin. The N-terminal region is shown in yellow and the amphipathic α-helix is indicated with a bracket. EGF-like repeats and CUB domains are shown in light and dark green, respectively. The truncated CUB domains in the cubilin minireceptor are shown in pale green. B) Schematic presentation of the structure of AMN. The mutations in the endocytic FXNPXF signals in the cytoplasmic domain of AMN are indicated below.

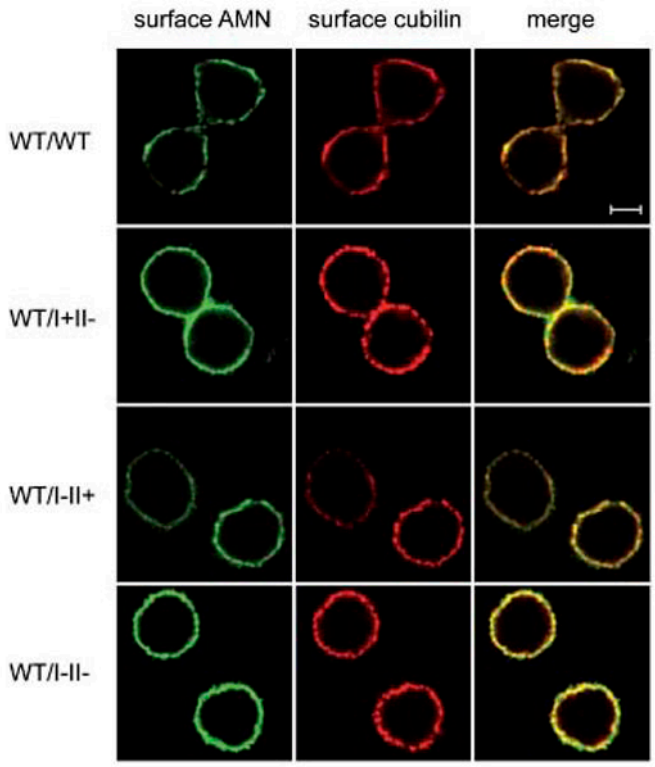


**Figure 2.**
Surface expression of AMN and cubilin in transfected CHO-K1 cells. Immunofluorescent analyses of the surface expression of cubilin and AMN in the WT, I−II+, I+II− and I−II− cell lines. Non-permeabilized cells were stained at 4°C resulting in staining of surface proteins only with a monoclonal anti-AMN antibody (shown in green) and a polyclonal anti-cubilin antibody (shown in red). The third panel shows a merged AMN and cubilin staining. Representative single confocal sections are shown. Scale bar = 5 μm.

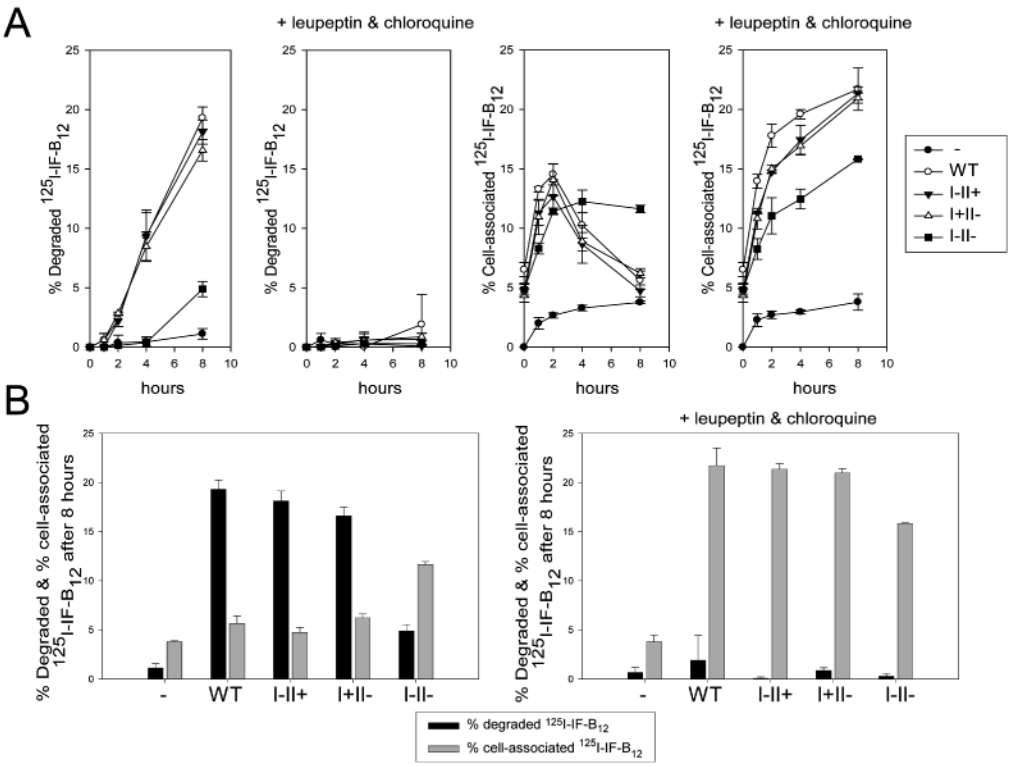


**Figure 3. Uptake of $^{125}$I-IF-$B_{12}$ in AMN-negative cells (−) and the WT, I−II+, I+II− and I−II− cell lines**

A) Cells were incubated with $^{125}$I-IF-$B_{12}$ for 0, 1, 2, 4 and 8 h at 37°C. Upon incubation with ligand, growth medium was removed and cells were solubilized. Degradation was measured as the cell-mediated increase in TCA-soluble radioactivity in the growth medium and cell-associated ligand by the radioactivity in the cell lysate. In the I−II− cells, a significant decrease at all times in the amount of degraded $^{125}$I-IF-$B_{12}$ was observed, while the I−II+ and I+II− cells practically were unaffected by the mutations. Addition of the lysosomal inhibitors, chloroquine and leupeptin, completely inhibited degradation of $^{125}$I-IF-$B_{12}$. B) Degraded (black bars) and cell-associated (gray bars) $^{125}$I-IF-$B_{12}$ after 8 h of incubation at 37°C without (left panel) and with (right panel) the lysosomal inhibitors, chloroquine and leupeptin. A significantly higher amount of cell-associated ligand is observed in the I−II− cells after 8 h (left panel).

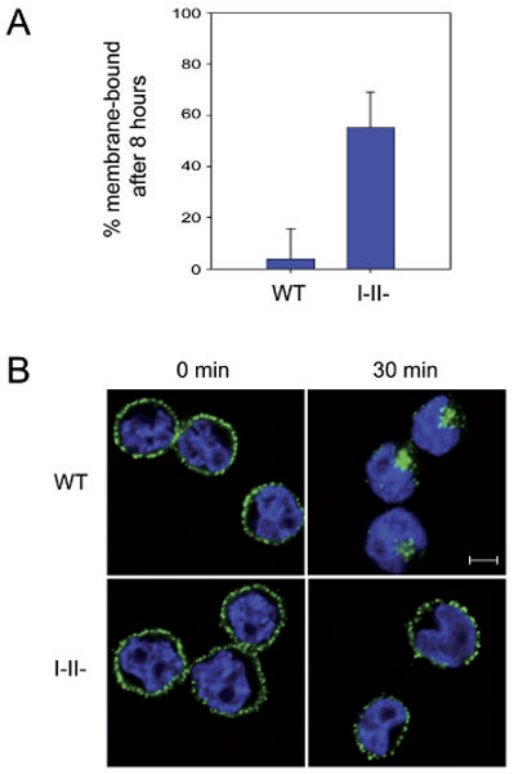


**Figure 4. Slower internalization rate in I−II− cells**

A) Membrane-bound $^{125}$I-IF-$B_{12}$ in the WT and **I−II−** cell lines. Cells were incubated with $^{125}$I-IF-$B_{12}$ for 8 h at 37°C. Upon incubation with ligand, cells were washed with 20 m M EDTA in PBS, pH 7.4 to remove membrane-bound $^{125}$I-IF-$B_{12}$. The percentage of membrane-bound $^{125}$I-IF-$B_{12}$ was found as the difference between EDTA-washed and unwashed cells in relation to the amount of cell-associated $^{125}$I-IF-$B_{12}$: % membrane-bound = [(cell-associated $^{125}$I-IF-$B_{12}$- cell-associated $^{125}$I-IF-$B_{12}$ after EDTA-treatment)/cell-associated $^{125}$I-IF-$B_{12}$] * 100%. B) Immunofluorescence microscopy analyses of internalization in WT and I−II− cell lines. Cells were incubated with anti-cubilin for 1 h at 4°C to saturate all receptor binding sites at the cell surface. Excess antibody was washed off and cells were subsequently incubated for 0 and 30 min at 37°C. Cells were visualized by nuclear DAPI-staining, and cubilin is stained green. Representative single confocal sections are shown. In both cell lines, surface labeling of cubilin is seen at 0 min. After 30 min, cubilin had been cleared from the cell surface and was found intracellularly in the WT cells, while no change was seen in the I−II− cells, indicating that these cells have an impaired ability to internalize. Scale bar = 5 μm.

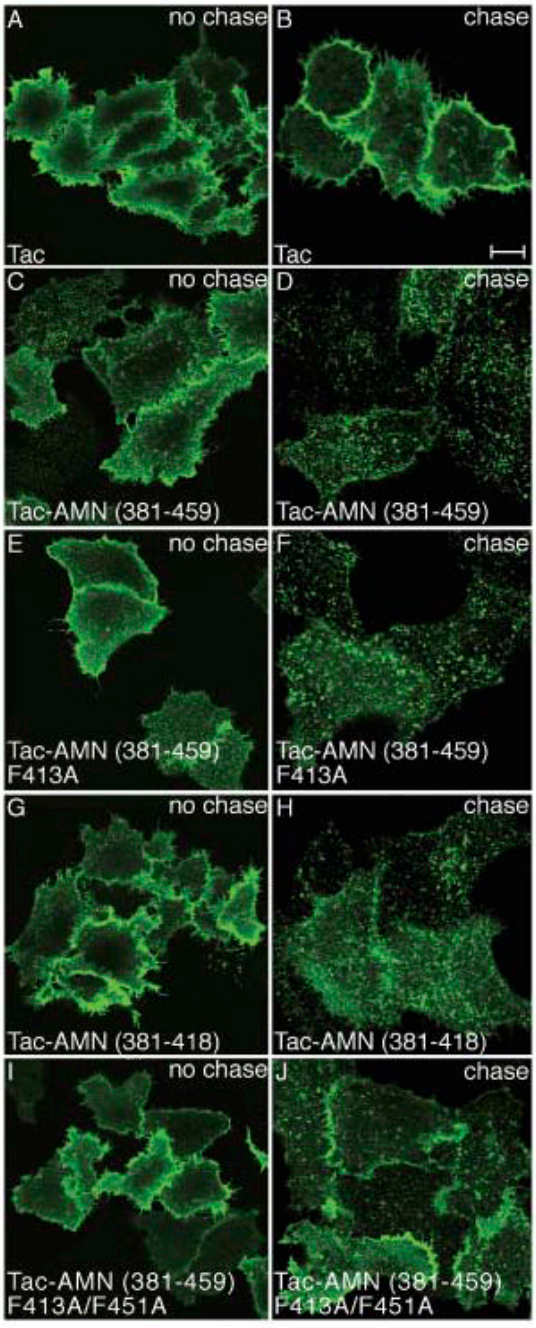


**Figure 5.**

Both FXNPXF motifs can mediate internalization of Tac-AMN. HeLa SS6 cells transiently transfected with the indicated Tac-AMN chimeras or Tac alone were surface labeled with anti-Tac antibody at 4°C. Following labeling, cells were either fixed immediately (no chase, panels A, C, E, G and I) or warmed to 37°C for 6–7 min and then fixed (chase, panels B, D, F, H and J). Following fixation, cells were permeabilized and stained with Alexa488 conjugated secondary antibody. Representative single confocal sections are shown. Note that there is a dramatic increase in the surface accumulation and a concomitant decreased internalization of Tac-AMN chimera harboring F→A mutations in both FXNPXF motifs (Tac-AMN-F413A-F451A-381–459; panel J) compared to other Tac-AMN chimeras

following chase. Also note that Tac or Tac-AMN (381–459) F413A/F451A chimera is not recruited to punctate structures (compare A and I with C, E and G) that are presumably clathrin-coated buds. Scale bar = 10 μm.

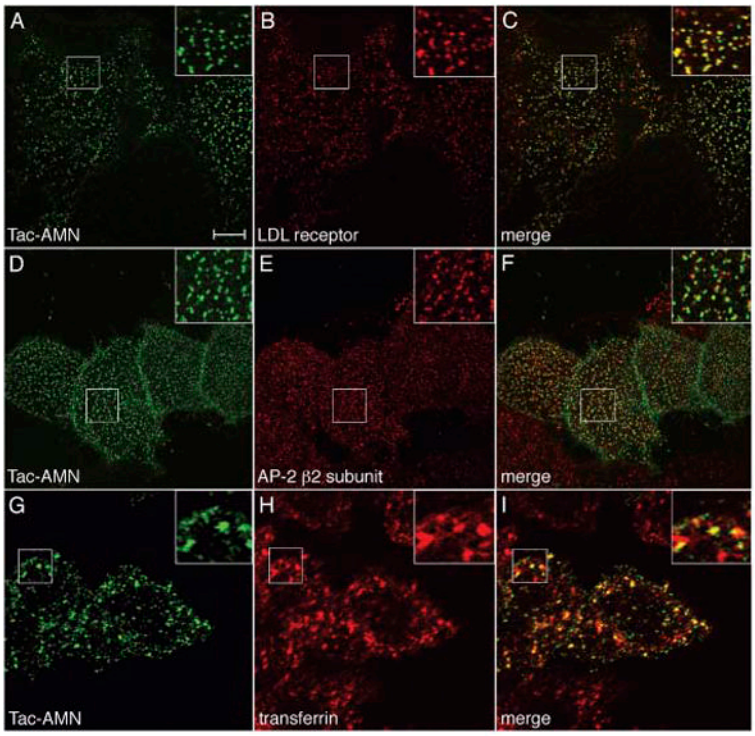


**Figure 6.**

Colocalization of Tac-AMN with markers of clathrin-dependent endocytic pathway. HeLa SS6 cells transfected with Tac-AMN were cultured in DMEM supplemented with 10% LPDS (A–C) or 10% FCS (D–I) overnight. (A–C) Cells were surface labeled with anti-Tac and anti-LDL receptor antibodies and fixed. (D–F) Cells were surface labeled with anti-Tac antibody alone, permealized briefly with digitonin then fixed and immunostained with anti-AP-1/2 GD/1 antibody. (G–I) Cells were serum starved for 1 h and then surface labeled with anti-Tac and transferrin568, then switched to 37°C for 15 min and fixed. A representative single confocal section is shown. Tac-AMN is in green and anti-LDL receptor (A–C), AP-1/2 (D–F) and transferrin568 (G–I) are in red. Magnified image of the boxed region in each panel is shown in the inset. Note substantial colocalization of Tac-AMN with the LDL receptor, AP-1/2 and internalized transferrin. Scale bar = 10 μm.

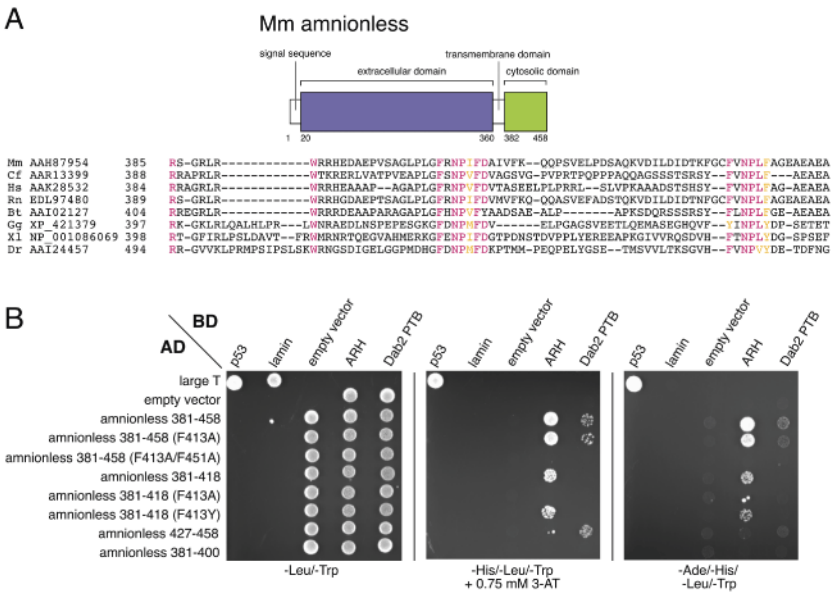


**Figure 7.**

Physical interaction between the AMN FXNPXF signals and PTB-domain CLASPs. A) Schematic illustration of the domain organization of Mus musculus (Mm) amnionless and primary sequence alignment of the cytosolic domains of AMN from mouse (Mm), Canis familiaris (Cf), Homo sapiens (Hs), Rattus norvegicus (Rn), Bos taurus (Bt); Gallus gallus (Gg); Xenopus laevis (Xl); Danio rerio (Dr). Accession numbers and starting residue numbers are indicated on the left. Identical residues are colored magenta while conservatively substituted residues are in yellow. Note the substantial phylogenetic differences within the intervening regions between the two core FXNPXF signals. B) S. cerevisiae strain AH109 transformed with the indicated pGBKT7 DNA binding domain (BD) or pGADT7 activation domain (AD) Gal4 fusion-encoding plasmids were selected and then equivalent aliquots spotted onto double (−Leu/−Trp), triple (−His/−Leu/−Trp) or quadruple (−Ade/−His/−Leu/−Trp) synthetic minimal medium plates and grown at 30°C.

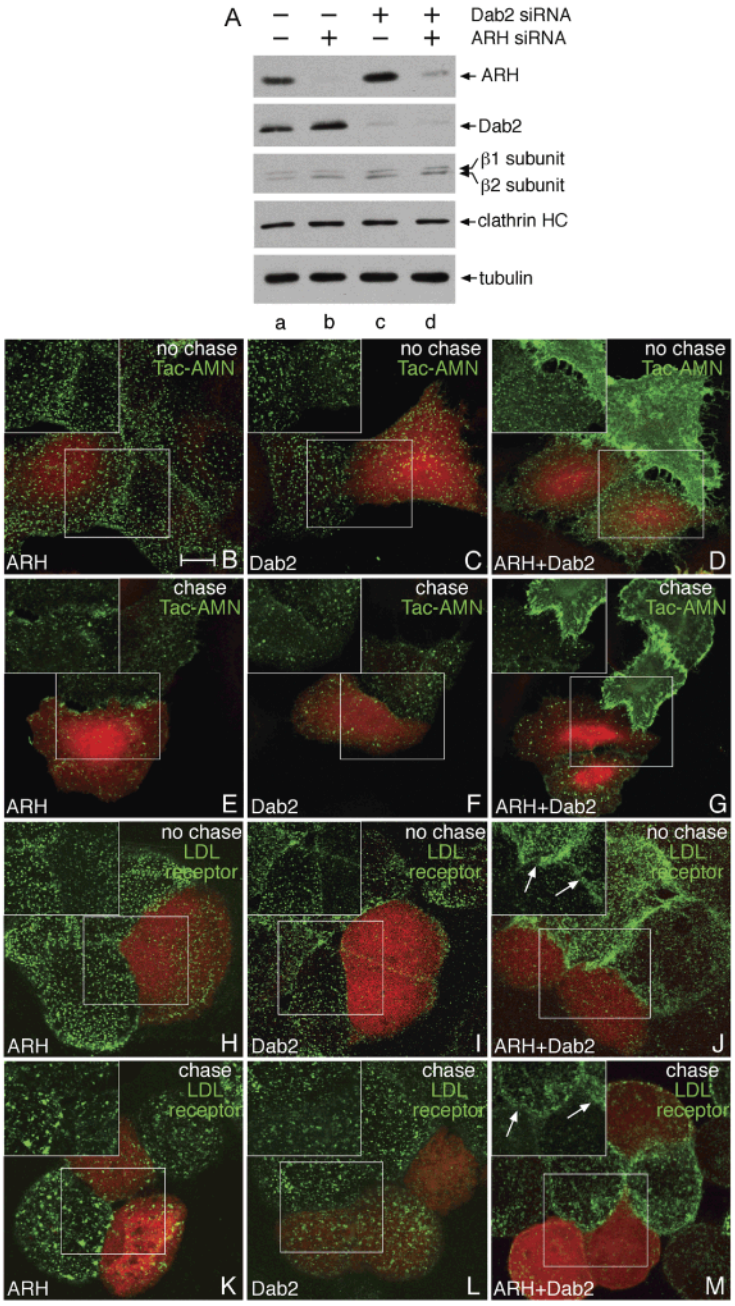


**Figure 8.**

Reduced internalization of Tac-AMN in ARH-and Dab2-depleted HeLa SS6 cells. A) Efficient siRNA-mediated depletion of ARH and/or Dab2 proteins. HeLa SS6 cells were either mock transfected (lane a) or transfected with specific siRNA duplexes targeting ARH and/or Dab2 (lanes b–d). After 48 h of transfection, cells were lysed, resolved by SDS–PAGE and immunoblotted with appropriate anti-ARH, anti-Dab2, anti-β1/β2, anti-clathrin and anti-tubulin antibodies. Note the efficient knockdown of only ARH and/or Dab2 in appropriate siRNA-treated cells. B–G) HeLa SS6 cells were either mock transfected or transfected with specific siRNA duplexes targeting ARH and/or Dab2. After 24 h, siRNA-treated cells were transfected with Tac-AMN, while mock-treated cells were co-transfected

with Tac-AMN and tdRFP. Six hours after the second series of transfections, mock-and siRNA-treated cells were trypsinized, mixed at 1:1 ratio and cocultured for 24 h. Cocultured cells were surface labeled with anti-Tac antibody and then either fixed immediately (no chase, panels B–D) or warmed to 37°C for 6–7 min and then fixed (chase, panels E–G), permeabilized and immunostained with Alexa488 conjugated secondary antibody. Representative single confocal sections are shown. Single-color images of the boxed region in each panel are shown in the inset. Cells expressing tdRFP fluorescence are mock treated. Note that there is a dramatic increase in the surface accumulation and decreased internalization of Tac-AMN in cells depleted of both ARH and Dab2. H–M) HeLa SS6 cells were either mock transfected or transfected with specific siRNA duplexes targeting ARH and/or Dab2. After 24 h siRNA-treated cells were transfected with lipofectamine alone, while mock-treated cells were transfected with tdRFP. After 6 h of second series of transfection, mock-and siRNA-treated cells were trypsinized, mixed at 1:1 ratio and cocultured for 24 h. Cocultured cells were either incubated with anti-LDL receptor IgG-C7 antibody at 4°C (no chase, panels H–J) or at 37°C (chase, panels K–M) for 15 min. Cells were fixed, permeabilized and stained with Alexa488 conjugated secondary antibody. Representative single confocal sections are shown. Single-color images of the LDL-receptor labeling in the boxed region in each panel are shown in the inset. Cells expressing tdRFP are mock treated. Note that there is a substantial increase in the surface accumulation of LDL receptors in cells depleted of both ARH and Dab2. Scale bar = 10 μm.

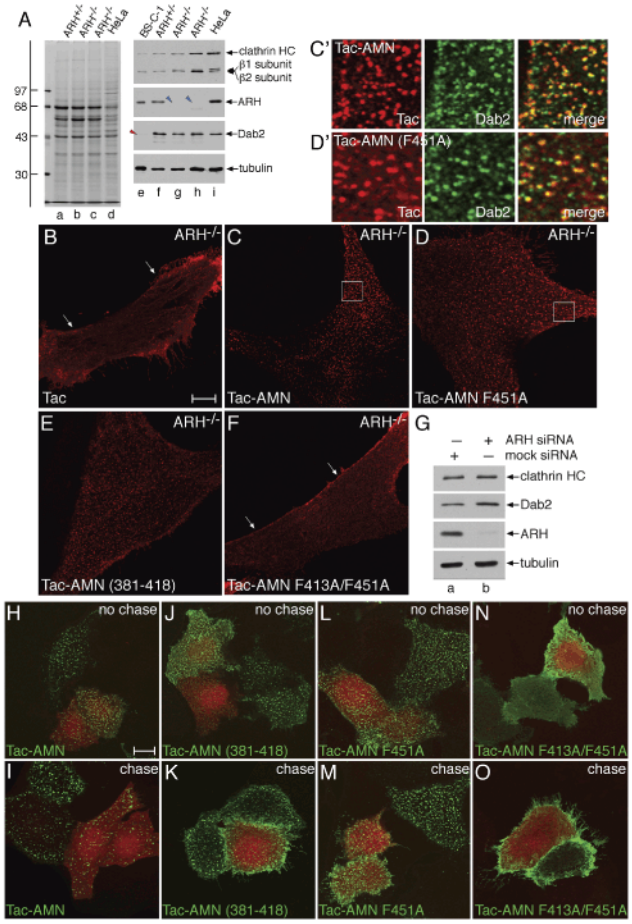


**Figure 9.**

Targeting of Tac-AMN and mutants to coated pits in ARH-null cells. A) Whole cell lysates from BS-C-1, ARH+/− (GM00695A), ARH−/− (GM00697) (35) or ARH−/− CK (34) fibroblasts and HeLa cells were resolved by SDS–PAGE and either stained with Coomassie Blue (left panel) or transferred to nitrocellulose. Portions of the blots were probed with appropriate anti-clathrin, anti-β1/β2, anti-ARH, anti-Dab2 or anti-tubulin antibodies, and only relevant regions are shown (right panel). Note that ARH is not detected in ARH−/− patient fibroblast lysates (blue arrowheads), while Dab2 is not detected in BS-C-1 cells (red arrowhead). The positions of the molecular weight markers are shown at the left. B–F) ARH −/− patient fibroblasts transiently transfected with Tac alone or the indicated Tac-AMN chimeras were fixed and surface labeled with anti-Tac antibody and refixed. Following permeabilization, cells were stained with anti-Dab2 antibody and appropriate Alexa-conjugated secondary antibodies. A representative single confocal section is shown. Note that in contrast to Tac (panel B) and Tac-AMN F413A/F451A (harboring mutations in both FXNPXF motifs; panel F), all other Tac-AMN chimeras (panels C, D and E) are targeted to punctate structures at the base of the cells (indicative of coated pits), which are also positive for Dab2 (boxed region in C and D are magnified in C′ and D′). G) HeLa SS6 cells were either mock transfected (lane a) or transfected with a SMART pool of specific siRNA duplexes targeting ARH (lane b). After 48 h of transfection, cells were lysed, resolved by SDS–PAGE and transferred to nitrocellulose. Portions of the blot were probed with appropriate anti-clathrin, anti-Dab2, anti-ARH and anti-tubulin antibodies, and only relevant regions are shown (top panel). Note efficient knockdown of only ARH in ARH-siRNA

treated cells. H–O) HeLa SS6 cells were either mock transfected or transfected with specific siRNA duplexes targeting ARH. After 24 h, siRNA-treated cells were transfected with indicated Tac-AMN chimeras, while mock-treated cells were co-transfected with tdRFP and indicated Tac-AMN chimeras. After another 6 h, appropriate Tac-AMN chimera and Tac-AMN chimera + tdRFP-transfected cells replated at a 1:1 ratio for an additional 24 h. Cocultured cells were surface labeled with anti-Tac antibody and then either fixed immediately (no chase; top panels) or warmed to 37°C for 6–7 min and then fixed (chase; lower panels), permeabilized and stained with Alexa 488-conjugated secondary antibody. Representative single confocal sections are shown. Cells with red fluorescence (expressing tdRFP) are mock siRNA-treated. Note that in contrast to the Tac-AMN F413A/F451A double mutant (N and O), the Tac-AMN (H and I), Tac-AMN (381–418) (J and K) and Tac-AMN F451A (L and M) chimeras are concentrated in punctate structures at the base of the cells and are internalized efficiently. Scale bar = 10 μm.